Physical properties of the magnetically frustrated very-heavy-fermion compound $YbCu_4Ni$

J. G. Sereni,[1] I. Čurlík,[2] M. Giovannini,[3] A. Strydom,[4,5] and M. Reiffers[2]

[1]*Department of Physics, CAB-CNEA, CONICET, 8400 San Carlos de Bariloche, Argentina*

[2]*Faculty of Humanities and Natural Sciences, University of Prešov, 17. novembra 1, Prešov, Slovakia*

[3]*Department of Physics and CNR-SPIN, University of Genova, Via Dodecaneso 31, Genova, Italy*

[4]*Highly Correlated Matter Research Group, Physics Department, University of Johannesburg, P.O. Box 524, Auckland Park 2006, South Africa*

[5]*Max Planck Institute for Chemical Physics of Solids, Nöthnitzerstrasse 40, D-01187 Dresden, Germany*

(Received 18 June 2018; revised manuscript received 1 August 2018; published 17 September 2018)

The physical properties of the very-heavy-fermion compound $YbCu_4Ni$ were characterized through structural, magnetic, thermal, and transport studies along nearly four decades of temperature ranging between 50 mK and 300 K. At high temperature, the crystal electric field level splitting was determined with $\Delta_1(\Gamma_6) = 85$ K and $\Delta_2(\Gamma_8) \approx 200$ K, the latter being a quartet in this cubic symmetry. An effective magnetic moment $\mu_{\rm eff} \approx 3\mu_B$ is evaluated for the Γ_7 ground state, while at high temperature the value for a Yb^{3+} ion is observed. At low temperature this compound shows the typical behavior of a magnetically frustrated system undergoing a change of regime at a characteristic temperature $T^* \approx 200$ mK into of Fermi-liquid-type "plateau" of the specific heat: $C_m/T|_{T\to 0} = \text{const}$. The change in the temperature dependence of the specific heat coincides with a maximum and a discontinuity in respective inductive and dissipative components of the ac susceptibility. More details about the nature of this ground state are revealed by the specific heat behavior under applied magnetic field.

DOI: 10.1103/PhysRevB.98.094420

I. INTRODUCTION

There is an increasing number of new Yb-based compounds which do not show long-range magnetic order down to the millikelvin range of temperature. Since they are characterized by having robust magnetic moments and by exhibiting a divergent increase of magnetic correlations in their paramagnetic phase upon cooling [1], it is expected that they belong to a different class of materials than those placed around a quantum critical point [2]. The strong increase in the density of magnetic excitations is reflected in power-law dependencies of the specific heat: $C_m(T)/T \propto 1/T^Q$, with exponents in the range $1 < Q \leqslant 2$ that clearly exceed the $C_m/T|_{T\to 0}$ values of usual non-Fermi liquids [3] that increase as $-\ln(T/T_0)$ with decreasing temperature. These compounds can be called very heavy fermions (VHFs) because their $C_m/T|_{T\to 0}$ range between $\approx$5 and $\approx$12 J/mol K^2 [4].

Two scenarios were proposed for the lack of long-range magnetic order in these compounds, one due to a very weak magnetic interaction between Yb ions and the other due to magnetic frustration. The former applies to $YbPt_2In$ and $YbPt_2Sn$ compounds that show the record high $\approx$12 J/mol K^2 value [5] after undergoing a maximum of $C_m(T)/T$ around 250 mK. Magnetic frustration can originate from peculiar geometric coordination of the magnetic moments [6] or from the competition between magnetic interactions of a different nature. Triangular (two-dimensional) and tetrahedral [three-dimensional (3D)] are the typical atomic configurations producing frustration at low temperature, with the striking feature that a number of Yb systems show a similar plateau of $C_m/T|_{T\to 0} = 7.5 \pm 0.5$ J/mol K^2 below a deviation from their power-law dependence of $C_m/T(T)$ within the millikelvin range [4] at a characteristic temperature T^*.

The mentioned absence of magnetic order in these VHFs was verified by different types of measurements besides specific heat. For example, the electrical resistivity ρ of $YbCu_{5-x}Au_x$ [1] and $PrInAg_2$ [7] decreases continuously with temperature around T^* without showing any discontinuity in their thermal slopes after undergoing a broad maximum. The lack of magnetic order in $YbCu_{5-x}Au_x$ down to 0.02 K was confirmed through nuclear quadrupole resonance and muon spin resonance (μSR) measurements [8].

A relevant aspect of the VHF compounds concerns their potential application for adiabatic demagnetization refrigeration based upon the large amount of entropy accumulated below 1 K that can be removed under magnetic field. This property was thoroughly explored in at least two compounds: $YbPt_2In$ [9] and $(Yb_{1-x}Sc_x)Co_2Zn_{20}$ [10]. The latter, $YbCo_2Zn_{20}$ [11], together with YbBiPt [12] belongs to the mentioned class of compounds showing similar $C_m/T|_{T\to 0} \approx 7.5$ J/mol K^2 below T^*. After having recognized the $YbCu_{5-x}Au_x$ ($0.4 \leqslant x \leqslant 0.7$) family as belonging to this "plateau"-type group while the stoichiometric compound $YbCu_4Au$ presents a cusp in the specific heat at $T \approx 0.8$ K [13], we have searched for an alternative composition in order to identify the main property producing such a different behavior. With this aim we have studied the physical properties of the isotypic compound $YbCu_4Ni$, which has nearly isochoric Ni atoms with an $\approx$3% smaller metallic radius than Cu, instead of Au, which is $\approx$20% larger.

II. EXPERIMENTAL DETAILS

The polycrystalline samples of $YbCu_4Ni$ and $LuCu_4Ni$ were prepared after weighing stoichiometric amounts of the

TABLE I. Structural parameters of $YbCu_4Ni$ refined from x-ray data in the space group F-43m. Residual values: $R_B = 4.10\%$, $R_F = 5.58\%$, $R_{WP} = 6.86\%$.

Atom	Site	x	y	z
Yb	4c	0.25	0.25	0.25
Cu	16c	0.6259(1)	0.6259(1)	0.6259(1)
Ni	4c	0	0	0

elements with the following nominal purity: Yb, -99.9% mass; Lu, 99.9% mass; Cu, 99.999% mass; and Ni, 99,995% mass. Then the elements were enclosed in small tantalum crucibles and sealed by arc welding under pure argon. The samples were melted in an induction furnace under a stream of pure argon. To ensure homogeneity during the melting, the crucibles were continuously shaken. The samples were then annealed in a resistive furnace for two weeks at 700 °C and finally quenched in cold water.

The two samples, $YbCu_4Ni$ and $LuCu_4Ni$, were characterized by optical and electron microscopy and by quantitative electron probe microanalysis. The crystal structure was examined by x-ray diffraction using Kα radiation. Rietveld matrix full-profile refinements were performed using the program FULLPROF [14].

Specific heat measurements on $YbCu_4Ni$ were carried out in a commercial physical property measurement system within the temperature range $0.4 < T < 300$ K in zero and applied magnetic fields up to 9 T. Using the same device, the temperature dependence of electrical resistivity was measured within the mentioned ranges of temperature and field for magnetoresistance. The low-temperature resistivity measurements (50 mK $< T <$ 4 K) were performed using a four-coil configuration, applying an ac current of 0.2 mA with a $f = 18.3$ Hz frequency. The temperature dependence of magnetization and magnetic susceptibility were obtained using a commercial magnetic property measurement system. At low temperature (between 50 mK and 4 K) ac magnetic susceptibility was measured while applying an excitation intensity of 1 Oe using different frequencies: $f = 4$, 1, and 0.1 kHz.

III. EXPERIMENTAL RESULTS

A. Crystal structure of $YbCu_4Ni$

Single-phase sample material of $YbCu_4Ni$ was obtained that showed a fcc structure of $MgCu_4Sn$ type (ternary derivative of the $AuBe_5$-type structure) with lattice constant $a = 6.943$ Å. The structural results of the Rietveld profile fitting are summarized in Table I, and the corresponding diffraction pattern is shown in Fig. 1(a). The structure was checked with respect to ordered and disordered locations of atoms in the structure, but the compound turned out to be a fully ordered compound with a full occupation of the atoms in each site. As depicted in Fig. 1(b), this fcc lattice can be viewed as a network of edge-sharing tetrahedra with Yb magnetic ions located at the vertices [15] being a 3D analog of a triangular lattice. The details of the structural refinement for the isotypic $LuCu_4Ni$ compound were reported in a previous work [16].

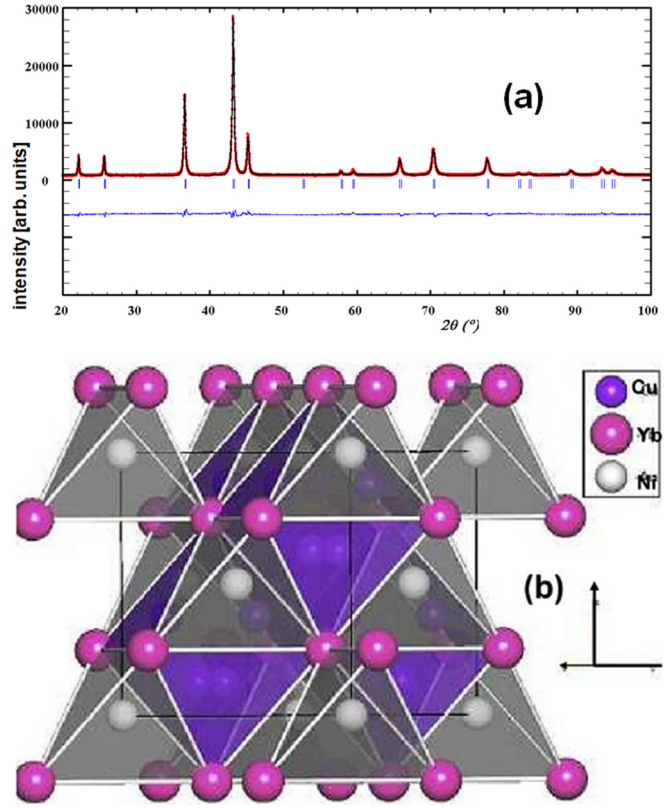

FIG. 1. (a) The experimental x-ray diffraction powder pattern of $YbCu_4Ni$ compared with the calculated diffraction diagram. The experimental data are shown by symbols, whereas the line through the data represents the results of the Rietveld refinement. The lower curve is the difference curve. The ticks indicate Bragg peak positions. (b) Crystal structure seen as edge-sharing tetrahedra with Yb ions located at the vertices (unit cell indicated by black lines) after [15].

B. Magnetic susceptibility and magnetization

In Fig. 2(a) the inverse magnetic susceptibility $(1/\chi)$ of $YbCu_4Ni$ is shown between 2 and 400 K. This temperature dependence can be described by a simple Curie-Weiss law with a negligible Pauli-type contribution ($\chi_0 = 4 \times 10^{-4}$ emu/mol Oe): $\chi(T) = C_c/(T + \theta_P) + \chi_0$. The Curie constant C_c extracted from a fit of the high-temperature range, 70–300 K, reveals an effective magnetic moment $\mu_{\text{eff}} = 4.42\mu_B$, close to the free Yb^{3+} ion value. The paramagnetic Curie-Weiss temperature $\theta_P = -19$ K indicates a dominating antiferromagnetic exchange at high temperature and a weak Kondo effect affecting the excited crystal electric field (CEF) levels. Below $T = 70$ K, $1/\chi$ turns down due to a smaller μ_{eff} value of the ground state (GS), which in the range $5 \geqslant T \geqslant 2$ K is evaluated as $\mu_{\text{eff}}^{\text{GS}} \approx 3.1\mu_B$ with a weak intensity of the molecular field $\theta_P^{\text{GS}} = -1.3$ K.

Below 4 K the magnetic susceptibility was measured by an ac method down to 50 mK, without detecting any frequency dependence. The results for $f = 4$ kHz, included in the inset in Fig. 2(b), show a maximum in the inductive component $\chi'(T)$ at $T_{\text{max}}^{\chi} \approx 170$ mK and a clear step in the dissipative component χ'' at the same temperature. This feature will be discussed in the following section together with the onset of coherence in $\rho(T)$ and the $C_m(T)/T|_{T\to 0}$ plateau. The

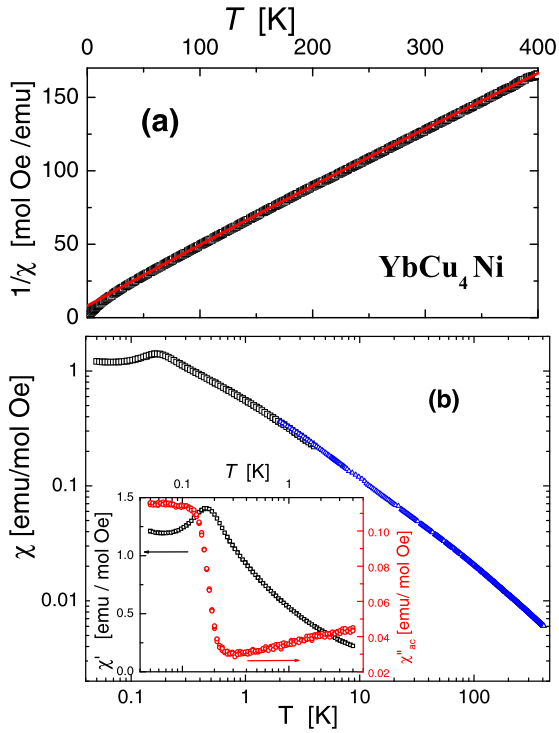

FIG. 2. (a) High-temperature dependence of the inverse magnetic susceptibility and (b) low-temperature inductive component of ac susceptibility scaled with high-temperature dc susceptibility in a double logarithmic representation. Inset: inductive (χ', left axis) and dissipative (χ'', right axis) components of ac susceptibility measured at $f = 4$ kHz in a semilogarithmic representation.

low-temperature $\chi'(T)$ dependence overlaps with the high-temperature χ_{DC} in Fig. 2(b) within 2 to 4 K, using the coincident thermal slope as a matching criterion; note the double-logarithmic representation.

The magnetization measurements performed between 2 K and room temperature while applying magnetic field up to 9 T are presented in Fig. 3. The strong curvature observed at $T = 2$ K can be described by the usual Brillouin function $B_J(x)$, with $x = B/T$ and effective $J = 1/2$.

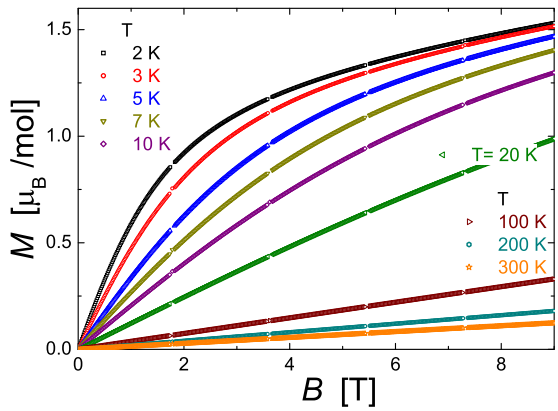

FIG. 3. Magnetization measurements versus field up to 9 T performed between 2 K and room temperature.

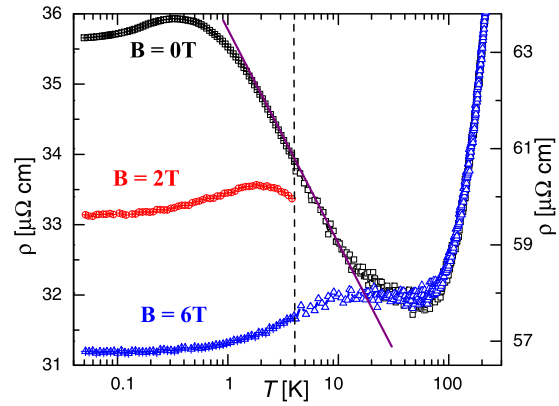

FIG. 4. Logarithmic temperature dependence of the electrical resistivity within four decades of temperature at $B = 0$ and 6 T, measured in different cryostats. The dashed vertical line indicates the data matched at $T = 4$ K using a ratio of 1.8 in the form factor (see the text). The straight purple line remarks the logarithmic T dependence in the range $2 < T < 10$ K. The $\rho(T \leqslant 4, B = 2T)$ K data are included to show the $T^{\rho}_{\max}$ variation with field.

C. Electrical resistivity and magnetoresistance

The temperature dependence of the electrical resistivity $\rho(T)$ of $YbCu_4Ni$ is presented in Fig. 4 within four decades of temperature at zero and $B = 6$ T, taking the high-temperature data from [17]. Since these results were obtained in different cryostats and from different pieces of the polycrystalline sample, a ratio of 1.8 between respective form factors is observed (compare the left low-temperature axis with the right high-temperature axis in Fig. 4). Such a difference is attributed to a different electrical connectivity between grains within the sample. Between room temperature and $T \approx 60$ K, $\rho(T)$ decreases mostly due to the decreasing phonon contribution. Then, below $T \approx 10$ K, $\rho(T)$ shows a typical $\rho(T) \propto -ln(T/T_0)$ Kondo increase for the $B = 0$ data.

After undergoing a broad maximum, centered at $T^{\rho}_{\max} \approx 350$ mK in the $B = 0$ data, $\rho_0|_{T\to 0}$ flattens. Magnetic field induces negative magnetoresistance at low temperature, while $T^{\rho}_{\max}$ is shifted to higher temperature. Low-temperature $\rho(T \leqslant 4$ K) data, measured with $B = 2$ T, are included to confirm this field-dependent tendency, which seems to be proportional to B.

D. Magnetic contribution to the specific heat

Figure 5 shows the high-temperature dependence of the $YbCu_4Ni$ specific heat. Since measured specific heat is usually dominated by electron band (C_{el}), phonon (C_{ph}), and magnetic (C_m) contributions, $C_P = C_{el} + C_{ph} + C_m$. In order to subtract the nonmagnetic components, $C_{el} + C_{ph} = \gamma T + \beta T^3$, we have investigated also the $LuCu_4Ni$ isotype. Its specific heat was also measured within $0.4 \leqslant T \leqslant 300$ K and is included in Fig. 5. Both compounds are close to reaching the expected Dulong-Petit values at high temperature. At low temperature, the extracted electron Sommerfeld coefficient for $LuCu_4Ni$ is γ(Lu) = 9.5 mJ/mol K^2, a typical value for nonmagnetic lanthanide compounds. Its Debye temperature

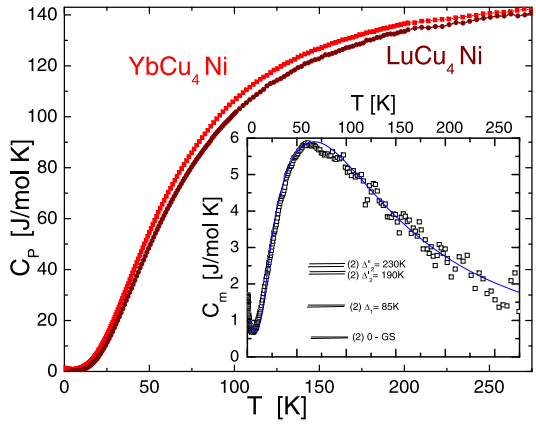

FIG. 5. Specific heat temperature dependencies up to room temperature of $YbCu_4Ni$ and $LuCu_4Ni$. Inset: high-temperature magnetic contribution and a fit accounting for the CEF levels and GS contributions.

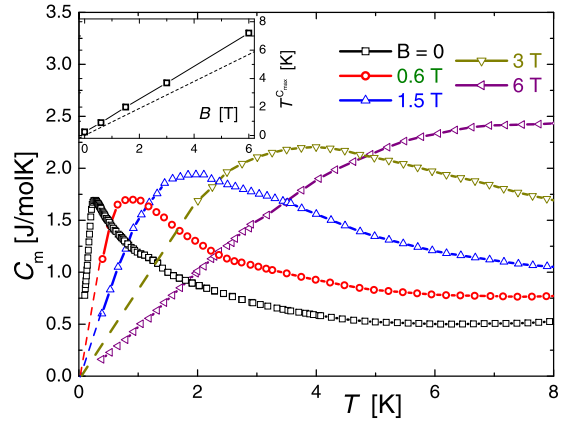

FIG. 6. Low-temperature dependencies of the specific heat of $YbCu_4Ni$ under different magnetic fields, 0–6 T. Inset: field dependence of the temperature of respective $C_m(T)$ maxima $T^{C_{\max}}$. The dashed line shows values computed applying the $T^{C_{\max}} \propto B$ formula for the Γ_7 doublet (see the text), and the solid curve shows the actual $C_m(T, B)$ observed maxima.

$\theta_D = 325\,\mathrm{K}$, was computed from the $\beta \approx 0.5\,\mathrm{mJ/mol\,K^4}$ coefficient.

At the low-temperature limit (i.e., $T < 0.2\,\mathrm{K}$), the specific heat measurements of $YbCu_4Ni$ show a clear increase attributed to the nuclear contribution C_n. Since this increase is found to proceed as $C_n = A_n/T^2$, in order to compute its contribution we plot the measured data using a $C_P/T = A_n/T^3 + C_m(T)/T$ temperature dependence. From the fit performed on the studied sample below $T = 0.22$ K we extract $A_n = 1.35 \times 10^{-3}\,\mathrm{J\,K/mol}$ and $C_m/T|_{T\to 0} = 7.5\,\mathrm{J/mol\,K^2}$. This A_n coefficient is very similar to the one obtained for $YbCu_{5-x}Au_x$ [1] and the value $C_m/T|_{T\to 0} = 7.5\,\mathrm{J/mol\,K^2}$ places $YbCu_4Ni$ in the class of VHF showing a plateau at $T \to 0$ [4]. No specific heat jump is observed in $C_m(T)$; rather, there is a well-defined cusp at $T^{C_{\max}} \approx 270\,\mathrm{mK}$ (as depicted in Fig. 8 below).

IV. DISCUSSION

A. Crystal electric field effect

In the inset of Fig. 5 one can see that $C_m(T)$ starts to increase around 10 K once the GS contribution is overcome by that of the excited CEF levels. This Schottky-type anomaly, centered at ≈60 K, is attributed to the Yb excited CEF levels. In a cubic symmetry, the eightfold ($N = 2J + 1 = 8$) degenerate ground state given by Hund's rule for a $J = 7/2$ angular moment splits into two doublets (Γ_6 and Γ_7) and a quartet (Γ_8) according to the calculations of Lea, Leask, and Wolf (LLW) [18]. In order to extract the level spectrum, we have fitted the experimental results applying a series of Schottky formulas to account for the contribution of respective excited CEF levels:

$$C_{\mathrm{CEF}}(T) = R\Sigma_i\left[\left(\frac{\Delta_i}{T}\right)/2\cosh\left(\frac{\Delta_i}{2T}\right)\right]^2, \qquad (1)$$

with R being the gas constant and Δ_i being the energy of the respective levels.

According to the result, the first excited doublet is located at $\Delta_1 = 90\,\mathrm{K}$, while the second corresponds to the quartet Γ_8 at double the energy: $\Delta_2 \approx 210\,\mathrm{K}$. Strictly, the fitting curve included in the inset of Fig. 5 also contains the actual GS contribution (see Fig. 6 for more detail) and an improvement obtained by splitting the Γ_8 quartet into two doublets at $\Delta_2' = 190\,\mathrm{K}$ and $\Delta_2'' = 230\,\mathrm{K}$. This further splitting mimics an eventual level broadening evaluated around 30 K. This value is in agreement with the observed $\theta_P = -19\,\mathrm{K}$ obtained through an extrapolation from $T \geqslant 70\,\mathrm{K}$, where the Γ_8 quartet becomes dominant and a Kondo screening effect may be detected. We remark that specific heat results allow us to identify the Γ_8 quartet as the most excited level because of its larger degeneracy. Although for a more precise determination of the respective CEF level energies complementary inelastic neutron scattering measurements are recommended, we remark that the relevant information is that the energy of the first excited CEF doublet is large enough to guarantee the treatment of the ground state as an isolated doublet.

Interestingly, the CEF level distribution in $YbCu_4Ni$ has some similarity to that of the isotypic $YbCu_{5-x}Au_x$; basically, because Γ_8 is the upper level [1], the energy distribution of the levels is quite different. This feature can be attributed to the different electronic characters between the electronlike Au and the holelike Ni ligands that present a point charge of opposite sign among them that clearly modifies the Coulomb potential, although without affecting the local structural symmetry.

B. About the doublet ground state

The same reason that allows us to identify the Γ_8 quartet as the most excited level, i.e., its larger degeneracy, impedes us from distinguishing between doublets Γ_6 and Γ_7 as the ground and first excited levels. An analysis based on relative degeneracies and levels splitting [19] applied to the LLW tabulations for $J = 7/2$ [18] gives two equivalent possibilities for the LLW parameter: $z = 0.5$ for a Γ_7 GS and $z = -0.3$ for the corresponding Γ_6 GS. However, according to previous calculations of the effective moment for those different pseudospin-1/2 doublets [20] $\mu_{\mathrm{eff}}(\Gamma_7) = 2.96\mu_B$ nearly

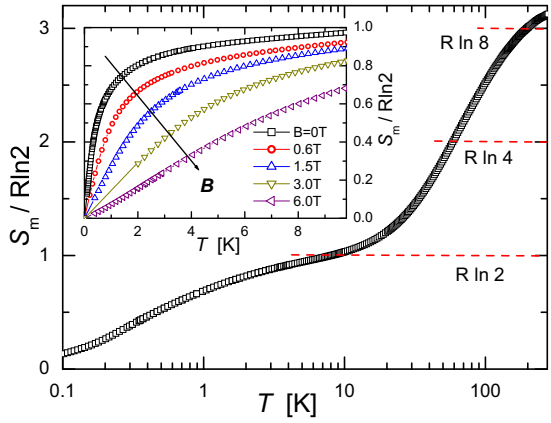

FIG. 7. The temperature dependence of the magnetic entropy of $YbCu_4Ni$ in a logarithmic temperature scale. The inset shows the entropy gain with different applied fields, in linear temperature scale.

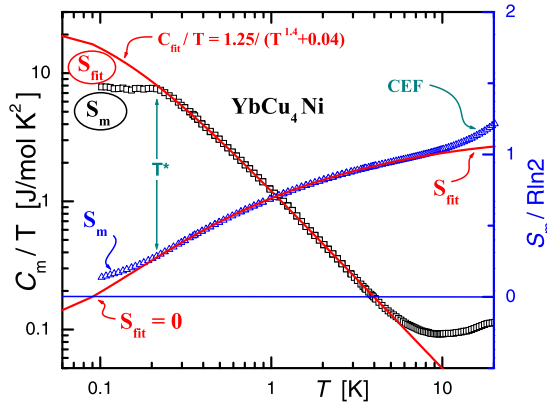

FIG. 8. Comparison between measured $C_m(T)/T$ and fitted $C_{\rm fit}/T|_{T>T^*}$ (solid curve) dependencies referred to the left axis in double-logarithmic representation. On the right axis (linear scale), the temperature dependencies of respective entropies are referred, showing how $S_{\rm fit} \to 0$ at $T > 0$. The value of $S_{\rm fit}(T \to \infty) = \mathrm{R}\ln 2$ is taken as the reference for the doublet GS. CEF indicates the onset of the excited crystal field level contribution above about 3 K.

coincides with the experimentally observed value rather than $\mu_{\rm eff}(\Gamma_6) = 2.31\mu_B$. This result can be checked by computing the expected saturation magnetization: $M_{\rm sat} = g_{\rm eff} J_{\rm eff} \mu_B$. For $g_{\rm eff}(\Gamma_7) = 3.43$ and $J_{\rm eff} = 1/2$ (for the doublet GS), we get $M_{\rm sat}(\Gamma_7) = 1.72\mu_B$, which can be expected from the $M(B)$ curve at $T = 2\,\mathrm{K}$ included in Fig. 3(a) with respect to $M_{\rm sat}(\Gamma_6) = 1.33\mu_B$.

C. Magnetic field effect

The effect of applied magnetic field on the temperature dependence of specific heat sheds further light on the GS nature through the Zeeman splitting dependence on $g_{\rm eff}$. The field dependence in $YbCu_4Ni$ is presented in Fig. 6 within the $0.4 \leqslant T \leqslant 8\,\mathrm{K}$ range and fields up to 6 T. The $C_P(T, B = 0)$ maximum $T^{C_{\max}} \approx 270\,\mathrm{mK}$, shifts to higher temperature in proportion to the field intensity, as shown in the inset of Fig. 6. Despite the fact that $C_P(T, B = 0)$ is closer to a Kondo-like anomaly than to a Schottky one (see Fig. 9 below), it is expected that the spin-up and spin-down components split by magnetic field tend to a Schottky anomaly at high enough field, i.e., $\mu B \gg k_B T$ [21]. From this criterion, based on the Zeeman splitting of the GS levels, we can confirm its Γ_7 GS nature by applying the $T^{C_{\max}} = 0.42 g_{\rm eff} B(\mu_B/k_B)$ relation [22] to obtain the dashed line in the inset of Fig. 6, taking $g_{\rm eff}(\Gamma_7) = 3.43$. Similar magnetic field effects on $C_m(T, B)$ are also in the cubic $Yb_{0.24}Sn_{0.76}Ru$ [20] ternary compound, where short-range magnetic order was claimed to explain the $C_m(T)$ anomaly centered at $T^{C_{\max}} \approx 0.9\,\mathrm{K}$. In the case of $YbCu_4Ni$ the pure Zeeman regime is reached once the magnetic energy μB overcomes the GS condensation energy characterized by $k_B T^*$ (the meaning of the T^* temperature will be discussed in Sec. IV D). Above that threshold the $C_m(T)$ anomaly tends to the Schottky type.

D. Entropy

The magnetic entropy gain S_m of $YbCu_4Ni$ along the full range of temperature is displayed in Fig. 7 in a logarithmic temperature scale. It is computed from the magnetic contribution to the specific heat as $S_m = \int (C_m/T)\, dT$.

At room temperature, the entropy slightly exceeds the expected value for the eightfold-degenerate $J = 7/2$ Hund's rule GS of Yb^{3+}, $S_m = R\ln 8 = 17.28\,\mathrm{J/mol\,K}$. This excess of entropy is probably due to an underevaluation of the phonon contribution at high temperature. The flattening of $S_m(T)$ around 10 K observed in Fig. 7 corresponds to $S_m = R\ln 2$, indicating that the doublet GS is well separated from the first excited CEF level at $\Delta_1 = 85\,\mathrm{K}$.

At low temperature, the change in curvature observed below $T \approx 300\,\mathrm{mK}$ can be analyzed accounting for the constraints imposed on the entropy by the Nernst postulate (third law of thermodynamics) [23]. For such a purpose we compare in Fig. 8 the temperature dependence of the specific heat with the entropy. In the double-logarithmic representation of the latter we may appreciate that $C_m(T > T^*)/T$ increases obeying a power-law dependence $\propto 1.25/(T^{1.4} + 0.04)\,\mathrm{J/mol\,K^2}$ which, below $T^* = 210\,\mathrm{mK}$, transforms into a plateau with $C_m/T|_{T\to 0} \approx 7.5\,\mathrm{J/mol\,K^2}$. The power-law dependence, plateau, and T^* values are similar to those reported for $YbCu_{4.3}Au_{0.7}$ [1].

The area marked as S_m in Fig. 8 represents the entropy computed from the measured specific heat that corresponds to the actual entropy released by the system upon cooling, whereas the area indicated as $S_{\rm fit}$ is extracted from $S_{\rm fit} = \int (C_{\rm fit}/T)\, dT$, where $C_{\rm fit}/T = 25/(T^{1.4} + 0.04)\,\mathrm{J/mol\,K^2}$ is the fitted power-law dependence above $T = T^*$. As a mathematical function, $C_{\rm fit}/T$ keeps growing below T^*, as depicted in Fig. 8, and therefore, the associated entropy exceeds the physical limit of "$R\ln 2$" for a doublet GS. The S_m and $S_{\rm fit}$ entropy trajectories are compared (right axis). Since the maximum entropy for a doublet GS is $R\ln 2$, the $S_{\rm fit}$ trajectory (solid curve) is drawn in Fig. 8 taking that value as the high-temperature limit. As expected, $S_{\rm fit}$ and S_m coincide within the fitting range (i.e., above T^*), with $S_m(T)$ for $T > 10\,\mathrm{K}$ being due to the onset of the excited CEF level contribution. On the low-temperature side, both entropy trajectories also split but due to different reasons. Since the physical system obeys the Nernst postulate: $S|_{T\to 0} \geqslant 0$, $S_m(T)$ is constrained

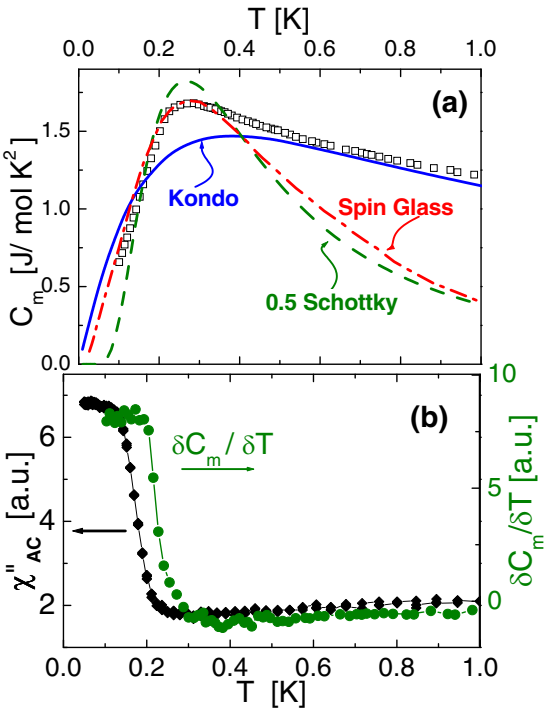

FIG. 9. (a) Low-temperature thermal dependence of the magnetic contribution to the specific heat $C_m(T)$. The solid curve shows theoretic prediction for a Kondo $S = 1/2$ impurity [25]. The dashed curve shows the Schottky anomaly divided by a factor 2, and the dash-dotted line shows an exemplary spin-glass system [22]. (b) Comparison between the $\chi''(T)$ jump (left axis) and that of the $C_m(T)$ derivative $\partial C_m/\partial T$ (right axis).

to change its trajectory and to point to $S_m = 0$ at $T = 0$. Otherwise it would become zero as $S_{\rm fit}$ does at finite temperature ($\approx$100 mK in this case). Since that change of trajectory is compelled by thermodynamic principles, T^* characterizes the temperature at which this sort of 'entropy bottleneck' occurs [24].

E. Ground-state properties

Apart from the discussion about the type of doublet CEF GS (Γ_7 or Γ_6) the $C_m(T)$ anomaly centered at $T^{C_{\rm max}} \approx 270$ mK poses a question about the nature of the GS below that maximum. In Fig. 9(a) the measured $C_m(T)$ dependence around the maximum is compared with some specific heat anomalies frequently observed in intermetallic systems [22]. One of them corresponds to a pure Schottky anomaly for a 1/2 pseudospin, which can be ruled out because it is much sharper than the measured $C_m(T)$ [notice that in Fig. 9(a) the included curve is half of the computed Schottky function]. Another possibility is given by a spin-glass behavior, which also results in a sharper curve above the maximum, whereas it nearly coincides below the maximum. Nevertheless, random short-range magnetic correlations related to the frustrated character of this system cannot be excluded, although to detect and evaluate the role of these microscopic mechanisms spectroscopic techniques such as low-T neutron diffraction and μSR are required.

The third comparison refers to the Kondo effect for a spin-1/2 Kondo impurity [25] with $T_K = 0.84$ K, which shows a similar T dependence below the maximum and only $\approx$15% difference from the observed $C_m(T)$ maximum. We should note that all these mechanisms coincide, showing a $C_m(T) \propto 1/T^2$ dependence at high temperature that differs from the power law extracted from the fit presented in Fig. 8.

From this comparison we infer that the thermal dependence of the specific heat of $YbCu_4Ni$ is not properly described by any of these well-identified anomalies. Nevertheless, its similarity to the Kondo-type behavior at $T < T^{C_{\rm max}}$ and $T > T^{C_{\rm max}}$ suggests the presence of some type of local fluctuations. In a more detailed analysis of the observed GS properties we see that there is a continuous formation of a sort of coherent behavior in $\rho(T)$ around $T = T^*$, as can be appreciated in Fig. 4 together with the absence of a jump in $C_m(T^*)$. These two features may suggest a Fermi-liquid (FL) character of the GS; however, the cusp of $\chi'(T)$ around that temperature and the clear step of $\chi''(T)$ [see the inset in Fig. 2(b)] disagree with the continuous Kondo condensation that characterizes a FL GS state formation.

The mentioned behavior of $\chi'(T)$ and $\chi''(T)$ around T^* announces a change of regime at that temperature, which does not correspond to a second-order phase transition because no $C_m(T)$ jump is observed. Although a maximum in dc $\chi(T)$ susceptibility is usually attributed to an antiferromagnetic transition, in an ac $\chi'(T)$ measurement a decreasing signal may also be due to an increasing decoupling between the ac field excitation and the magnetic moments' dynamic response. This feature is correlated with energy dissipation below the $\chi'(T)$ maximum which is actually observed in the $\chi''(T < T^*)$ signal as a steplike thermal dependence [see Fig. 9(b)]. To gain insight into this unusual scenario we have investigated further derivatives of the free energy G and found that the $\partial C_m/\partial T$ discontinuity at T^* gently coincides with that of $\chi''(T)$, as can be appreciated in Fig. 9(b). This fact indicates that the system undergoes a change between $G(T)$ minima but in a continuous way.

In magnetically frustrated systems it was proposed [24] that the free energy shows a peculiar behavior because the entropy trajectory is compelled to change at T^*, obeying the Nernst postulate, as was discussed in Sec. IV D. In this context, the $G(T)$ minimum of the paramagnetic phase blurs out due to the *entropy bottleneck* produced by the divergent power-law growth of the density of excitations. Thus, the $G(T > T^*)$ minimum is not feasible anymore for $T \to 0$, and consequently, the system slides along the free-energy surface into any other accessible minimum. In the case of the compounds identified by the plateau-type behavior, $T < T^*$ $G(T)$ minimum is characterized by a constant density of excitations, notably with a coincident $C_m/T|_{T\to 0} = 7.5 \pm 0.5$ J/mol K^2 value. Whether these excitations have a continuous energy spectrum like in a Fermi liquid or one that is a sort of liquid of spin excitations has to be determined by spectroscopic techniques.

V. SUMMARY

Based on the parent compound $YbCu_5$, we have replaced one Cu atom with Ni to obtain the stoichiometric and

atomically well ordered compound $YbCu_4Ni$ with a lattice parameter $a = 6.9429$ Å in its cubic structure. At high temperature the rare-earth atom exhibits localized $4f$ electron nature with an effective magnetic moment close to Yb^{3+} according to the Hund's eightfold GS. The CEF splits the $J = 7/2$ multiplet into well-defined doublets as the GS and first excited state, while the expected quadruplet exhibits a moderate broadening.

At low temperature, the Yb lattice shows clear signs of magnetic frustration, which is expected from its pyrochlore-type structure, which fulfils the conditions for a 3D geometrical frustration, providing the optimal requirements for this type of study in a stoichiometric compound. This scenario is reflected in a power-law increase of the specific heat with decreasing temperature. This diverging tendency is limited by the Nernst postulate that compels a change of regime, at a characteristic temperature $T^* \approx 200$ mK, which in this case corresponds to a plateau with a very high density of states: $C_m/T|_{T\to 0} = 7.5\,\mathrm{J/mol\,K^2}$. Simultaneously, electrical resistivity undergoes a broad maximum around 300 mK before flattening as $T \to 0$. Although both features point to the formation of a Fermi liquid, in this compound the GS does not form in a continuous way, as demonstrated by the discontinuity in the $C_m(T)$ slope and confirmed by a step in the dissipative component of the ac susceptibility at $T \approx T^*$.

Since this type of phenomenology is also observed in a number of Yb intermetallics showing a similar change of regime at T^*, with a coincident plateau value (see $YbCu_{5-x}Au_x$ [1], $PrInAg_2$ [7], $YbCo_2Zn_{20}$ [11], and YbBiPt [12]), it suggests that around T^* there is a common underlying physics that was discussed in detail in the present work in order to help eventual future theoretic approaches.

ACKNOWLEDGMENTS

M.R. and I.Č. are partially supported by projects VEGA 1/0956/17 and VEGA 1/0611/18. A.S. thanks the SA-NRF (93549) and the UJ URC/FRC for financial assistance. J.G.S. is partially supported by the SECTYP-Universidad Nacional de Cuyo project 06/C520.

[1] I. Čurĺik, M. Giovannini, J. G. Sereni, M. Zapotokova, S. Gabani, and M. Reiffers, Extremely high density of magnetic excitations at $T = 0$ in $YbCu_{5-x}Au_x$, Phys. Rev. B **90**, 224409 (2014).

[2] H. V. Löhneysen, A. Rosch, M. Vojta, and P. Wölfe, Fermi-liquid instabilities at magnetic quantum transitions, Rev. Mod. Phys. **79**, 1015 (2007).

[3] G. R. Stewart, Non-Fermi-liquid behavior in d- and f-electron metals, Rev. Mod. Phys. **73**, 797 (2001).

[4] J. G. Sereni, Entropy constraints in the ground state formation of magnetically frustrated systems, J. Low Temp. Phys. **190**, 1 (2018), and references therein.

[5] T. Gruner, D. Jang, A. Steppke, M. Brando, F. Ritter, C. Krellner, and C. Geibel, Unusual weak magnetic exchange in $YbPt_2Sn$ and $YbPt_2In$, J. Phys.: Condens. Matter **26**, 485002 (2014).

[6] R. Moessner and A. P. Ramirez, Geometrical frustration, Phys. Today **59**(2), 24 (2006).

[7] A. Yatskar, W. P. Beyermann, R. Movshovich, and P. C. Canfield, Possible Correlated-Electron Behavior from Quadrupolar Fluctuations in $PrInAg_2$, Phys. Rev. Lett. **77**, 3637 (1996).

[8] P. Carretta, R. Pasero, M. Giovannini, and C. Baines, Magnetic-field-induced crossover from non-Fermi to Fermi liquid at the quantum critical point of $YbCu_{5-x}Au_x$, Phys. Rev. B **79**, 020401(R) (2009).

[9] D. Jang, T. Gruner, A. Steppke, K. Mistsumoto, C. Geibel, and M. Brando, Large magnetocaloric effect and adiabatic demagnetization refrigeration with $YbPt_2Sn$, Nat. Commun. **6**, 8680 (2015).

[10] Y. Tokiwa, B. Piening, H. S. Jeevan, S. L. Bud'ko, P. C. Canfield, and P. Gegenwart, Super-heavy electron material as metallic refrigerant for adiabatic demagnetization cooling, Sci. Adv. **2**, e1600835 (2016).

[11] M. S. Torikachvili, S. Jia, E. D. Mun, S. T. Hannahs, R. C. Black, W. K. Neils, D. Martien, S. L. Bud'ko, and P. C. Canfield, Six closely related related YbT_2Zn_{20} heavy fermion compounds with large local moment degeneracy, Proc. Natl. Acad. Sci. USA **104**, 9960 (2007).

[12] Z. Fisk, P. C. Canfield, W. P. Beyermann, J. D. Thompson, M. F. Hundley, H. R. Ott, E. Felder, M. B. Maple, M. A. Lopez de la Torre, P. Visani, and C. L. Seamanet, Massive Electron State in YbBiPt, Phys. Rev. Lett. **67**, 3310 (1991).

[13] M. Galli, E. Bauer, St. Berger, Ch. Dusek, M. Della Mea, H. Michor, D. Kaczorowski, E. W. Scheidt, and F. Marabelli, Evolution of ground state properties of $YbCu_{5-x}Au_x$, Physica B **312–313**, 489 (2002).

[14] J. Rodríguez-Carvajal, Recent advances in magnetic structure determination by neutron powder diffraction, Physica B **192**, 55 (1993).

[15] M. Giovannini, I. Čurlík, F. Gastaldo, M. Reiffers, and J. G. Sereni, The role of crystal chemistry in $YbCu_{5-x}Au_x$, J. Alloys Compd. **627**, 20 (2015).

[16] I. Čurlík, M. Reiffers, and M. Giovannini, Study of magnetic contribution to the heat capacity of $YbCu_4Ni$, Acta Phys. Polonica A **122**, 3 (2012).

[17] I. Čurĺik S. Matosova, S. Ilkovic, M. Reiffers, and M. Giovannini, Transport and magnetic properties of $YbCu_4Ni$, Acta Phys. Pol. A **122**, 6 (2012).

[18] W. E. Lea, M. J. M. Leask, and W. P. Wolf, The raising of angular momentum degeneracy of f-electron terms by cubic crystal fields, J. Phys. Chem. Solids **23**, 1381 (1962).

[19] J. G. Sereni, Crystal field effects on the specific heat of $(La,Er)Al_2$, in *Crystal Field Effects in Metals and Alloys*, edited by A. Furrer (Plenum, New York, 1977), p. 309.

[20] T. Klimczuk, C. H. Wang, J. M. Lawrence, Q. Xu, T. Durakiewicz, F. Ronning, A. Llobet, F. Trouw, N. Kurita, Y. Tokiwa, H.-o. Lee, C. H. Booth, J. S. Gardner, E. D. Bauer, J. J. Joyce, H. W. Zandbergen, R. Movshovich, R. J. Cava, and J. D. Thompson, Crystal fields, disorder, and antiferromagnetic short-range order in $Yb_{0.24}Sn_{0.76}Ru$, Phys. Rev. B **84**, 075152 (2011).

[21] M. B. Maple, Superconductivity: A probe for the magnetic state of local moments in metals, Appl. Phys. **9**, 179 (1976).

[22] J. G. Sereni, Magnetic systems: Specific heat, in *Reference Module in Material Science and Material Engineering*, edited by S. Hashmi, Materials Science and Materials Engineering (Elsevier, Oxford, 2016), pp. 1–13.

[23] A. B. Pippard, A miscellany of useful ideas, in *Elements of Classical Thermodynamics* (Cambridge University Press, Cambridge, 1964).

[24] J. G. Sereni, Entropy Bottlenecks at $T \rightarrow 0$ in Ce-Lattice and Related Compounds, J. Low Temp. Phys. **179**, 126 (2015).

[25] H. U. Desgrages and K. D. Schotte, Specific heat of the Kondo model, Phys. Lett. A **91**, 240 (1982).